Materials Today Chemistry 40 (2024) 102199

Contents lists available at ScienceDirect

Materials Today Chemistry

journal homepage: www.journals.elsevier.com/materials-today-chemistry/

Regulation of molecular conjugation to realize mult-color room temperature phosphorescence of carbon dots in urea and ammonium pentaborate precursor matrices

Qing Yao [a], Yuan Wang [b], Minqiang Wang [a,*], Nikolai V. Gaponenko [c], Zheyuan Da [a], Jindou Shi [a], Chen Zhang [a], Junnan Wang [a]

[a] Electronic Materials Research Laboratory, Key Laboratory of the Ministry of Education International Center for Dielectric Research&Shannxi Engineering Research Center of Advanced Energy Materials and Devices, Xi'an Jiaotong University, 710049, Xi'an, PR China
[b] Center for Rare Earth & Vanadium & Titanium Materials, School of Materials Science & Engineering, Sichuan University, Chengdu, 610065, PR China
[c] Belarusian State University of Informatics and Radioelectronics, P. Browki 6, 220013, Minsk, Belarus

ARTICLE INFO

Keywords:
Carbon dots
Room temperature phosphorescent
Molecular conjugation

ABSTRACT

Carbon dots (CDs) room temperature phosphorescent (RTP) materials have great application prospects in optoelectronic devices, advanced anti-counterfeiting, information encryption and bio-imaging due to its excellent optical properties. However, achieving long-lifetime phosphorescence with color-tunable RTP CDs is a huge challenge. In this work, precursor molecules with different degrees of conjugation: 4-ethoxycarbonyl phenylboronic acid (4-EpBA), 9-phenanthracenylboronic acid (9-PhBA) and 1-pyrenylboronic acid (1-PyBA) were combined with urea and ammonium pentaborate (AP) matrix through high temperature pyrolysis method, long-lifetime and colorful phosphorescent CDs composites of 4-EpBA@Urea, 9-PhBA@Urea and 1-PyBA@AP were successfully synthesized. As the degree of conjugation of the precursor molecules increased, the phosphorescence colors of 4-EpBA@Urea, 9-PhBA@Urea and 1-PyBA@AP were blue, green and orange, respectively. In addition, since 1-PyBA@Urea could not produce orange phosphorescence emission, we chose 1-PyBA@AP that was able to generate bright orange phosphorescence after UV excitation. Furthermore, the rationality behind phosphorescence emission mechanism and wavelength modulation is further conformed by density functional theory (DFT) calculations. Finally, RTP CDs composites are successfully applied for advanced anti-counterfeiting and optical information storage.

1. Introduction

Afterglow materials have the advantages of long luminescence lifetime, large Stokes shift and the ability to emit light after the excitation light source is removed, which have been used in a variety of applications in sensing [1], anti-counterfeiting [2,3] and optoelectronic devices [4,5]. Through rational design and novel synthetic strategies to modulate spin–orbit coupling (SOC) and populate triplet exciton states (T_1), luminophores with long lifetimes and bright afterglow characteristics can be realized. Afterglow materials are typically categorized according to their luminescence mechanism, such as long-persistent luminescence (LPL), room temperature phosphorescence (RTP), or thermally activated delayed fluorescence (TADF) [6].

Carbon dots (CDs), as an emerging class of zero-dimensional carbon nanomaterials with good photostability, simple preparation process, low cost, good biocompatibility and low toxicity [7], are widely used in bio-imaging [8], electrochemical sensing [9–11], laser devices [12,13], opto-electronic devices [14]and so on. In addition, the afterglow properties of CDs have attracted much attention due to the advantage of being easily tunable in a variety of different matrices. They are mainly classified into three strategies: RTP, TADF and delayed fluorescence based on Förster resonance energy transfer [15]. Among them, there are two main strategies to realize the phosphorescence emission of CDs [16], one is the self-protection method: it is often adopted to enhance the phosphorescence emission of CDs by doping atoms such as B, N, F into the CDs to improve the efficiency of the intersystem crossing (ISC) from the singlet to the triplet state [17–19]. The second is the matrix-assisted method: the RTP of the CDs is generated or enhanced by

* Corresponding author.
E-mail address: mqwang@mail.xjtu.edu.cn (M. Wang).

https://doi.org/10.1016/j.mtchem.2024.102199
Received 9 May 2024; Received in revised form 28 June 2024; Accepted 12 July 2024
Available online 16 July 2024

embedding the CDs into various matrices, such as CDs@BA [20], CDs@PVA [21], CDs@SiO_2 [22], CDs@LDHs [23], CDs@zeolite [24] and so on. Currently, most of the RTP CDs are prepared in a complex process, with a short phosphorescence lifetime and difficulty in achieving color-tunable phosphorescence emission. CDs are often embedded in the framework structure of various inorganic matrices and form strong interactions with the matrices through the abundant functional groups on the surface to build stable triplet states and effectively realize afterglow properties. Among them, urea and boric acid are often used as precursor matrices for CDs to achieve phosphorescence emission [25–29]. Han et al. [30]. obtained 6.47 s ultralong-lifetime deep blue RTP CNQDs with a phosphorescence emission wavelength of 418 nm by embedding CNQDs into the tri-*s*-triazine framework based on urea as a precursor matrix, and also obtained green RTP CNQDs by increasing the conjugation of the precursor molecules. Although the CNQDs complexes reported in this work have excellent deep blue phosphorescence emission performance, the phosphorescence lifetime of the green RTP is suboptimal and fails to achieve red phosphorescence emission. Li et al. [31]. constructed a long lifetime and high-efficiency RTP emission system by suppressing the non-radiative transition process and promoting the triplet exciton of the phosphors using boric acid as the host matrix and organic phosphors as guest molecules. Blue, yellow-green and red phosphorescence emission were realized by precursor molecules with different conjugation degrees. This work realizes red phosphorescence emission, but its green phosphorescence is missing and the lifetime of yellow-green phosphorescence is much shorter than that of blue phosphorescence.

In this work, we synthesized long-lifetime multicolored RTP CDs by one-pot pyrolysis using 4-EpBA, 9-PhBA, and 1-PyBA with different degrees of conjugation, which were added to the precursor matrix of urea and AP, respectively, achieving deep blue, green and orange phosphorescence. Moreover, the blue and green phosphorescence lifetimes are longer than those of most RTP CDs that have been reported [32–34]. On the one hand, with increasing conjugation of 4-EpBA, 9-PhBA and 1-PyBA precursor molecules, the phosphorescence emission wavelengths of 4-EpBA@Urea, 9-PhBA@Urea and 1-PyBA@AP were realized to be red-shifted. On the other hand, since the RTP CDs synthesized with urea as the precursor matrix (CNQDs@Urea), the covalent bond types formed between the CNQDs and the matrix and the π-bond conjugation strengths of CNQDs were different, the 4-EpBA@Urea and 9-PhBA@Urea achieved longer-lifetime blue and green phosphorescence after UV light excitation compared with 4-EpBA@AP and 9-PhBA@AP. Besides, the RTP CDs synthesized with AP as the precursor matrix (CBNQDs@AP) have a high degree of densification between CBNQDs and a high degree of discrete π-orbital interactions compared with CNQDs@Urea, resulting in a low energy requirement for π-π* transition, and are more capable of achieving long-wavelength phosphorescence emission after UV excitation. Thus, 1-PyBA@AP exhibits significant orange phosphorescence emission properties. Moreover, the rationality behind phosphorescence emission mechanism and wavelength modulation is further conformed by density functional theory (DFT) calculations. Finally, the excellent phosphorescent properties of the synthesized samples were utilized to realize the application of anti-counterfeiting encryption and optical information storage.

2. Results and discussion

Briefly, 4-EpBA@Urea was synthesized by pyrolysis of 4-EpBA and urea at 200 °C for 3 h, similarly, 9-PhBA@Urea and 1-PyBA@Urea were obtained using a similar methodology. However, the synthesis of 4-EpBA@AP, 9-PhBA@AP and 1-PyBA@AP only required the substitution of the precursor matrix urea to AP (see details in the Experimental Section in Supporting Information) in Fig. 1a. Besides, the comparison of phosphorescence spectra for different raw material ratios, heating times and synthesis temperatures are shown in Fig. S1. The synthesized 4-EpBA@Urea was able to emit deep blue phosphorescence after the UV light was turned off and the RTP duration for more than 21 s to the naked eye. Excitingly, increasing the conjugation of the precursor molecules, 9-PhBA@Urea was able to emit green phosphorescence after UV light was removed, and the RTP duration for more than 18 s to the naked eye. In addition, by continuing to increase the conjugation of the precursor molecules and substituting the precursor matrix urea with AP, 1-PyBA@AP was able to emit orange phosphorescence with the RTP duration more than 3.5 s after the UV light was turned off in Fig. 1b.

In the scanning electron microscopy (SEM) image in Fig. S2a, it can be seen that 4-EpBA@Urea with urea as the precursor matrix presents a multilayered honeycomb fluffy structure, which indicated that the urea matrix can provide a good physical confinement feature. In the transmission electron microscopy (TEM) image we can see that the CNQDs are well embedded into the matrix framework structure (Fig. 2a and b), with an average particle size of 11.5 nm in Fig. 2c, which corresponds to the 0.19 nm crystal spacing of the (023) crystal plane of graphitic carbon nitride [35] (Fig. 2d). In addition, since 9-PhBA@Urea also utilized urea as a precursor matrix, the microscopic morphology exhibited the same characteristics as 4-EpBA@Urea. For 1-PyBA@AP, with AP as the precursor matrix, a tight multilayered lamellar structure can be seen in the SEM image in Fig. S2b. In the TEM image, CBNQDs can be observed dispersed in the matrix structure (Fig. 2e) with an average particle size of 2.8 nm in Fig. 2f. The larger average particle size and mutual spacing of CNQDs in 4-EpBA-Urea than CBNQDs in 1-PyBA@AP is attributed to the fact that more gases are generated during pyrolysis of urea rendering the matrix structure more fluffy, resulting in less restriction of the growth of the CNQDs and a higher degree of dispersion. Fig. 3a shows that the X-ray diffraction (XRD) pattern of CNQDs@Urea exhibits two distinct characteristic peaks at 12.7° and 28.2°, attributed to the

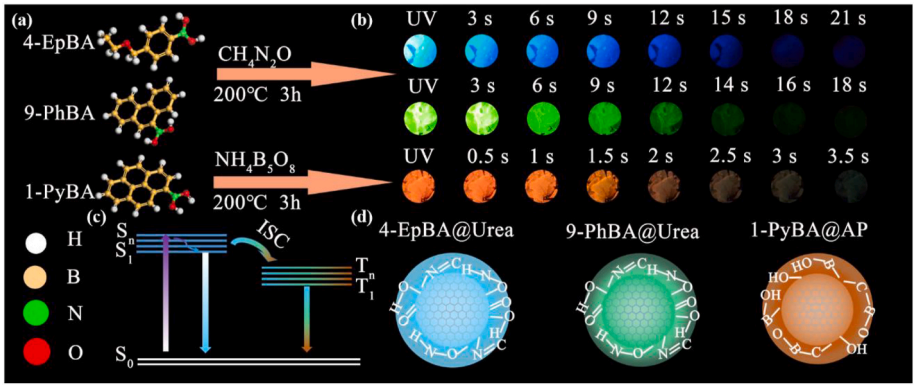

Fig. 1. a) Schematic illustration for synthesizing RTP CDs. b) Actual pictures after the UV light excitation is turned off. c) Possible fluorescence and phosphorescence emission processes. d) Phosphorescence emission mechanism schematic illustration.

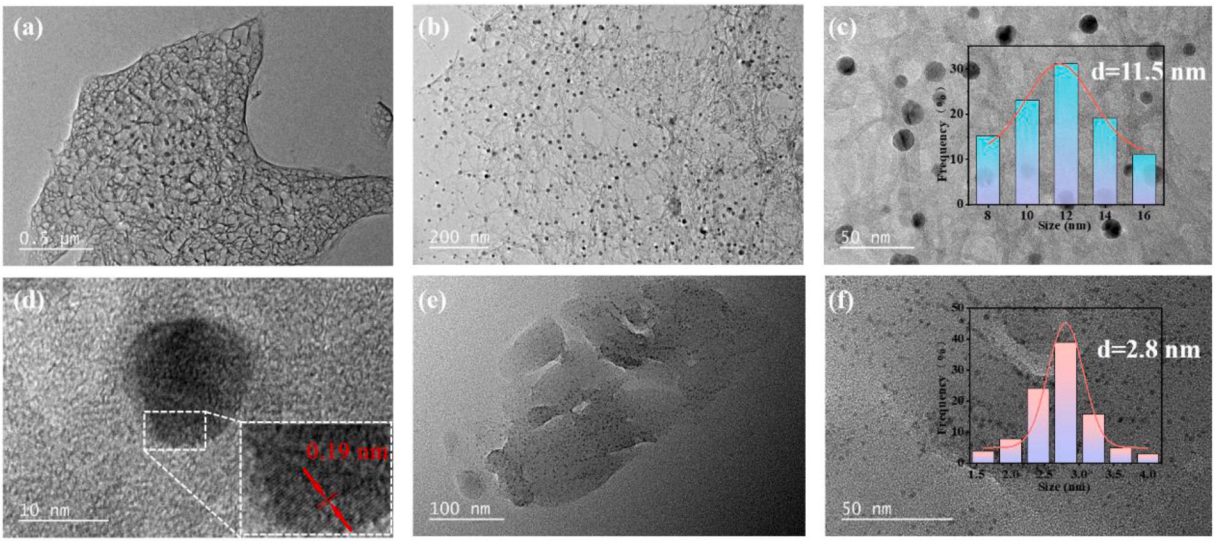

Fig. 2. a-c) The TEM images of 4-EpBA@Urea, inset is average particle size statistics. d) HRTEM image of 4-EpBA@Urea. e,f) TEM images of 1-PyBA@AP, inset is average particle size statistics.

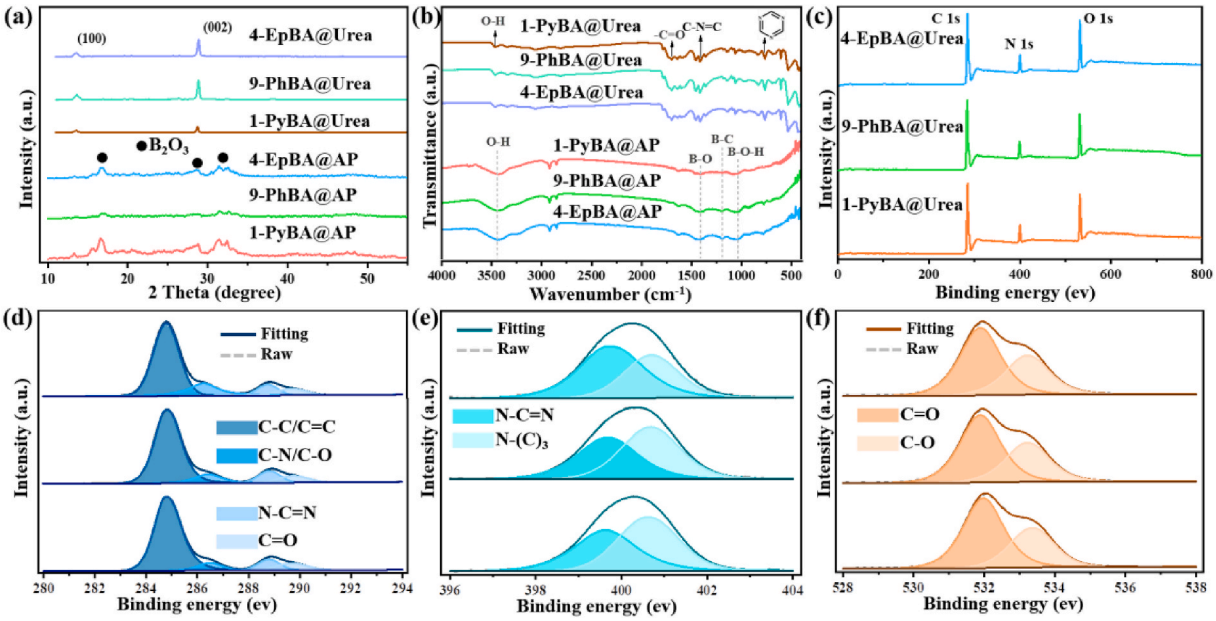

Fig. 3. a) XRD diffraction patterns and b) FT-IR patterns of CNQDs@Urea and CBNQDs@AP. c) XPS spectra of CNQDs@Urea. d, e, f) high-resolution XPS spectra of C 1s, N1s, O 1s.

periodically repeating tri-*s*-triazine unit indexed as the (100) crystal plane [36] and the stacking of the conjugated aromatic system indexed as the (002) crystal plane of graphitic carbon nitride [37,38], respectively. Therefore, it can be inferred that the CNQDs in CNQDs@Urea are well embedded in the tri-*s*-triazine skeletons, consistent with the results of TEM tests. It can be observed in Fig. 3a that the XRD patterns of CBNQDs@AP with three distinct characteristic peaks at 16.7°, 28.6° and 31.5° are attributed to B_2O_3 [39]. It also indicates that the intramolecular hydrogen bonds among AP molecules were destroyed at a high temperature, resulting in the occurrence of dehydration and condensation to form B_2O_3. Similarly, the CBNQDs in CBNQDs@AP are embedded in the B_2O_3 matrix, providing the necessary physical constraints for phosphorescence emission.

Fourier transform infrared spectroscopy (FT-IR) and X-ray photoelectron spectroscopy (XPS) are performed to further determine the functional groups and chemical composition of samples. The characteristic absorption peaks shown by CNQDs@Urea at 3465, 1700, 1420 and 762 cm^{-1} were attributed to the stretching vibrations of O–H, –C═O, C–N═C and triazine ring, respectively [40] in Fig. 3b. Besides, CBNQDs@AP showed O–H, B–O, B–C and B–O–H stretching vibrations at 3450, 1420, 1188 and 1042 cm^{-1} in Fig. 3b, respectively [41,42]. As shown in Fig. 3c, the XPS spectrum displays that CNQDs@Urea contains three elements: C, N and O. Fig. 3d shows that the high-resolution C1s spectrum deconvoluted to obtain four peaks at 284.8, 286.3, 288.8 and 289.8 eV, which are attributed to C–C/C═C, C–N/C–O, N–C═N and C═O [43], respectively. The high-resolution N1s spectrum (Fig. 3e) contains two peaks at 399.6 and 400.6 eV corresponding to C–N═C and N-$(C)_3$. The XPS spectrum of O1s (Fig. 3f) exhibits two peaks at binding energies of 531.8 eV (C═O) and 533.2 eV (C–O). It could be observed that 4-EpBA@Urea had higher C–N/C–O and N–C═N content compared to 9-PhBA@Urea and 1-PyBA@Urea in Fig. 3d. According to previous report [26], the C–N/C–O bonds on the surface of CDs are able to

generate new energy level structures and can promote the generation of the triplet excitons through n-π* transition, leading to stronger phosphorescence emission of 4-EpBA-Urea. The full scan XPS spectra (Fig. S3a) showed that 1-PyBA@AP contained four elements: B, C, N, and O. The high-resolution B1s spectrum (Fig. S3b) contains three peaks at 192.6, 193.3 and 194.5 eV, corresponding to BCO_2 surrounded by carbon–oxygen atoms, boron oxide and B—O bonds [44,45], respectively. As shown in Fig. S3c, the high-resolution C1s spectrum deconvoluted to obtain two peaks at 284.7 and 285.2eV, which are attributed to C–C/C═C and C–N/C–O, respectively. The XPS spectrum of N1s (Fig. S3d) exhibits two peaks at binding energies of 401.9 (N–H) and 402.7 eV (N–O). The high-resolution spectra of O 1s (Fig. S3e) show two peaks at 532.7and 533.6 eV for C═Oand C–O, respectively. Moreover, the XPS spectra of 4-EpBA@AP and 9-PhBA@AP were investigated to be the same as for 1-PyBA@AP in Fig. S4. Moreover, the Raman spectrum was exhibited in Fig. S5 and the Raman diffraction peaks position of 1-PyBA@AP is shifted towards lower wavelengths compared to 4-EpBA@Urea, which is caused by the increased conjugation of 1-PyBA@AP compared to 4-EpBA@Urea [46].

Fig. S6a shows the UV–vis absorption spectra of CNQDs@Urea, with a sharp peak at 222 nm and a broad peak at 285 nm corresponding to π-π* transition in the sp2-π conjugated structural domain and n-π* transition of C═N/C═O, respectively. Notably, the intensity of the UV absorption peak of 4-EpBA@Urea was much higher in the 240 nm–300 nm range, indicating that 4-EpBA@Urea has stronger phosphorescence emission when the excitation wavelength is in this region. The UV absorption spectra of CBNQDs@AP are exhibited in Fig. S6b, and it can be found that CBNQDs@AP has a significant red shift compared to CNQDs@Urea. This is due to the fact that when urea is used as the precursor matrix, pyrolysis generates a huge amount of gas making the matrix framework structure more fluffy. Thus, the small limitation on the growth of CNQDs, the large mutual spacing between CNQDs and the lower interactions of the discrete π orbitals cause weaker π-bonding conjugation, leading to the higher energy required for the π-π* transition. However, with AP as the precursor matrix, the CBNQDs are distributed densely to each other (which is consistent with the TEM test results in Fig. 2), the energy required for the π-π* transition is low, resulting in a red-shift of the UV absorption spectrum. It is noteworthy that 1-PyBA@Urea has almost no absorption at wavelengths >300 nm, whereas 1-PyBA@AP has a significant absorption at 300–400 nm, this is the reason for the different phosphorescence emission properties of 1-PyBA@Urea and 1-PyBA@AP under UV excitation.

The optimal fluorescence and RTP emission wavelengths for 4-EpBA@Urea were 325 and 430 nm, respectively, corresponding to an excitation wavelength of 250 nm in Fig. 4a. To further demonstrate the luminescence center of fluorescence and phosphorescence, the fluorescence spectra and phosphorescence mapping spectra of 4-EpBA@Urea at different excitation wavelengths were adopted in Fig. 4b and c. It can be concluded that both fluorescence and phosphorescence do not exhibit multiple emission centers, focused at 325 nm and 430 nm, respectively, which also suggests that neither fluorescence nor phosphorescence emission of 4-EpBA@Urea is dependent on the excitation wavelength. The maximum values of fluorescence and RTP emission wavelengths of 9-PhBA@Urea are 398 and 525 nm, corresponding to the excitation

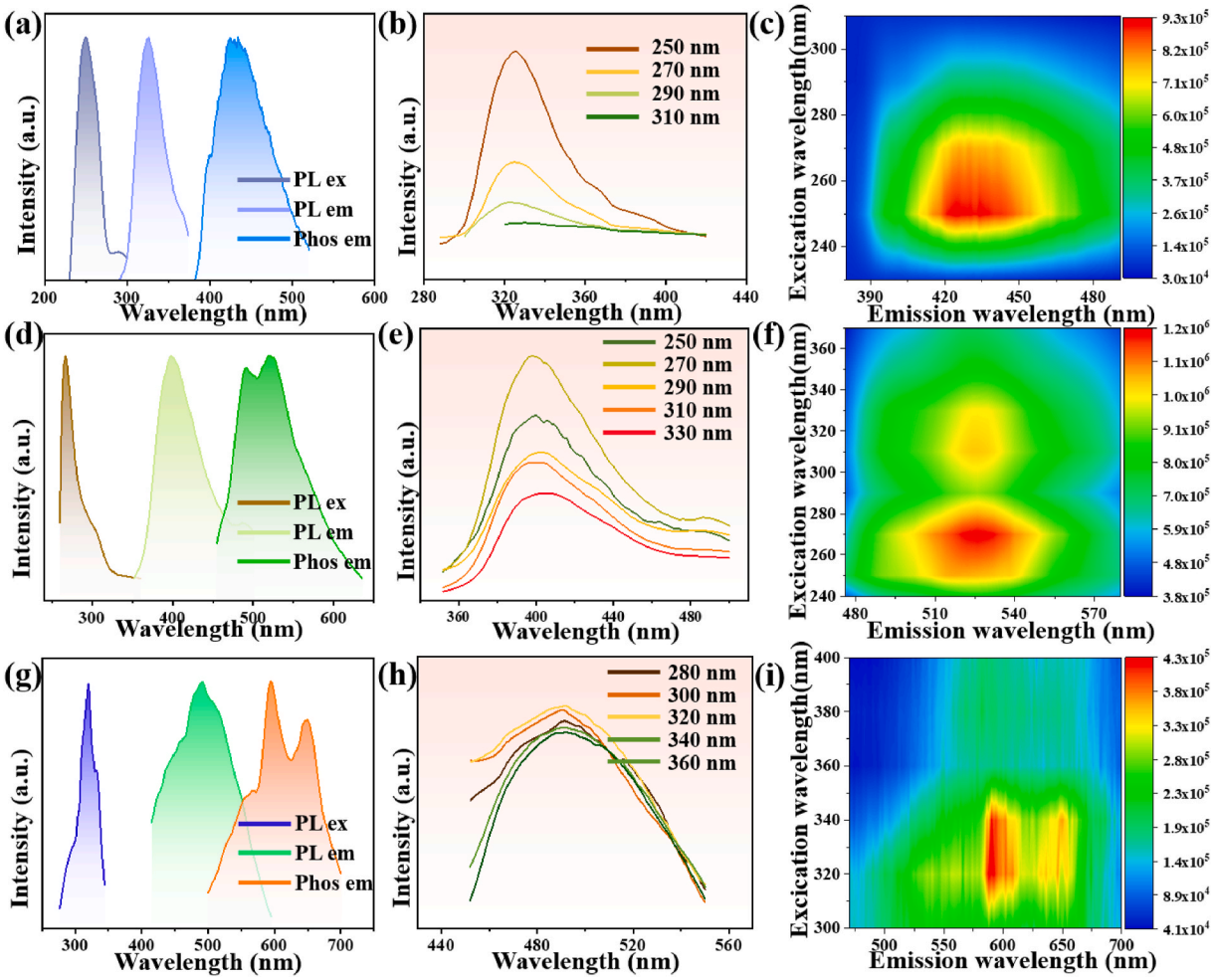

Fig. 4. a, d, g) Optimal excitation, fluorescence and phosphorescence mapping spectra of 4-EpBA@Urea, 9-PhBA@Urea and 1-PyBA@AP. b, e, h) Fluorescence spectra at different excitations. c, f, i) Spectral mapping of phosphorescence at different excitations.

wavelength of 267 nm in Fig. 4d. Furthermore, it was investigated that the fluorescence and phosphorescence emission of 9-PhBA@Urea was centered at 398 and 525 nm and that both fluorescence and phosphorescence emission were independent of the excitation wavelength in Fig. 4e and f. The optimal fluorescence emission wavelength of 1-PyBA@AP is 490 nm, and the optimal phosphorescence emission peaks are 590 and 650 nm, which correspond to the excitation wavelength of 320 nm (Fig. 4g). Similarly, both the fluorescence and phosphorescence emission of 1-PyBA@AP are independent of the excitation wavelength in Fig. 4h and i. The blue and green phosphorescence generated by 4-EpBA@AP and 9-PhBA@AP lasted for a shorter time than 4-EpBA@Urea, 9-PhBA@Urea, after the excitation of UV is turned off (as shown in Fig. 1b and Fig. S7) and the phosphorescence mapping spectra of 4-EpBA@AP and 9-PhBA@AP in Fig. S8 were exhibited. This is due to the binding of CNQDs to the tri-*s*-triazine framework, which possesses more covalent bonds that generate n-π* transitions (e.g., C═N/C═O), resulting in the promotion of more triplet state excitons compared to the B_2O_3 matrix. Thus, 4-EpBA@Urea and 9-PhBA@Urea have longer phosphorescence lifetimes. In addition, the phosphorescence color of 1-PyBA@Urea under UV of 330 nm excitation is blue-green and the phosphorescence lifetime is very short in Fig. S5, which is due to the low UV absorption intensity of 1-PyBA@Urea at 300–400 nm and its inability to satisfy the excitation wavelength required for orange phosphorescence emission. Therefore, we selected 1-PyBA@AP with high UV absorption intensity at 300–400 nm and can generate orange phosphorescence emission to meet the subsequent practical application scenarios.

As shown in Fig. 5a, the afterglow decay spectra of 4-EpBA@Urea, 9-PhBA@Urea and 1-PyBA@AP were tested, and the phosphorescence lifetimes were calculated to be 2.16, 1.87 and 0.36 s, respectively, according to the equation: $\tau_{avg} = \sum a_i\tau_i^2 / \sum a_i\tau_i$. The temperature-dependent spectra of 4-EpBA@Urea, 9-PhBA@Urea and 1-PyBA@AP were investigated as shown in Fig. 5b, c and d. It can be observed that the samples have the highest intensity of phosphorescence emission at 77 K, and their peak intensity decreases with increasing temperature, resulting from an effective restriction of vibrational motion and suppression of nonradiative transitions at low temperatures, which indicates their remarkable phosphorescence properties [47]. Furthermore, the phosphorescence lifetimes of 4-EpBA@Urea, 9-PhBA@Urea, and 1-PyBA@AP were tested to be 2.49, 1.96, and 0.39 s at 77 K, respectively, which were significantly longer than the 2.16, 1.87, and 0.36 s at 300 K (Fig. 5e). As shown in Fig. 5f, the CIE coordinates show the 4-EpBA@Urea, 9-PhBA@Urea and 1-PyBA@AP as (0.15, 0.03), (0.22, 0.62) and (0.60, 0.39), respectively, thus indicating that the phosphorescence colors of 4-EpBA@Urea, 9-PhBA@Urea and 1-PyBA@AP are blue, green and orange.

Since the use of urea and AP as precursor matrix conferred excellent RTP properties to 4-EpBA@Urea, 9-PhBA@Urea and 1-PyBA@AP during pyrolysis, we need to further investigate their RTP mechanism. Typically, under the excitation of UV light, the ground state (S_0) of CDs can absorb energy to transition to the excited state (S_1), and the excited state (S_1) returns to (S_0) to emit fluorescence [48] in Fig. 6b. Since covalent bonds such as O–H, N–C═N, B–O, etc. can be generated under the pyrolysis process impose restrictions on the vibration of the functional groups on the surface of the CDs, resulting in the transfer of the energy of the CDs from S_1 to T_1 (the ISC process) to create phosphorescence emission in Fig. 1c and d. Notably, the phosphorescence colors of 4-EpBA@Urea, 9-PhBA@Urea and 1-PyBA@AP were blue, green and orange, respectively. Furthermore, we calculated the structures of three molecules with different degrees of conjugation, 4-EpBA, 9-PhBA, and 1-PyBA, employing density-functional theory (DFT). The hybrid exchange-correlation density functional (B3LYP) together with the DEF2TZVP basis sets were utilized in conjunction with a Grim dispersion (D3) correction incorporating a Beck–Johnson (BJ) damping parameter to account for different noncovalent interactions [49]. Geometrical optimization and energy-gap calculations were performed on all three molecular structures. Fig. 6a presents the optimized geometrical models of these three molecular structures under vacuum conditions along with the electron distribution in their lowest unoccupied molecular orbital (LUMO) and highest occupied molecular orbital (HOMO). The band gaps of these three molecular structures on the computational surface are 5.331, 4.395, and 3.596 ev, respectively. Due to the gradual increase of conjugated fragments in 4-EpBA, 9-PhBA, and 1-PyBA, the formation of CDs is accompanied by the fusion of the sp2 carbon domains, resulting

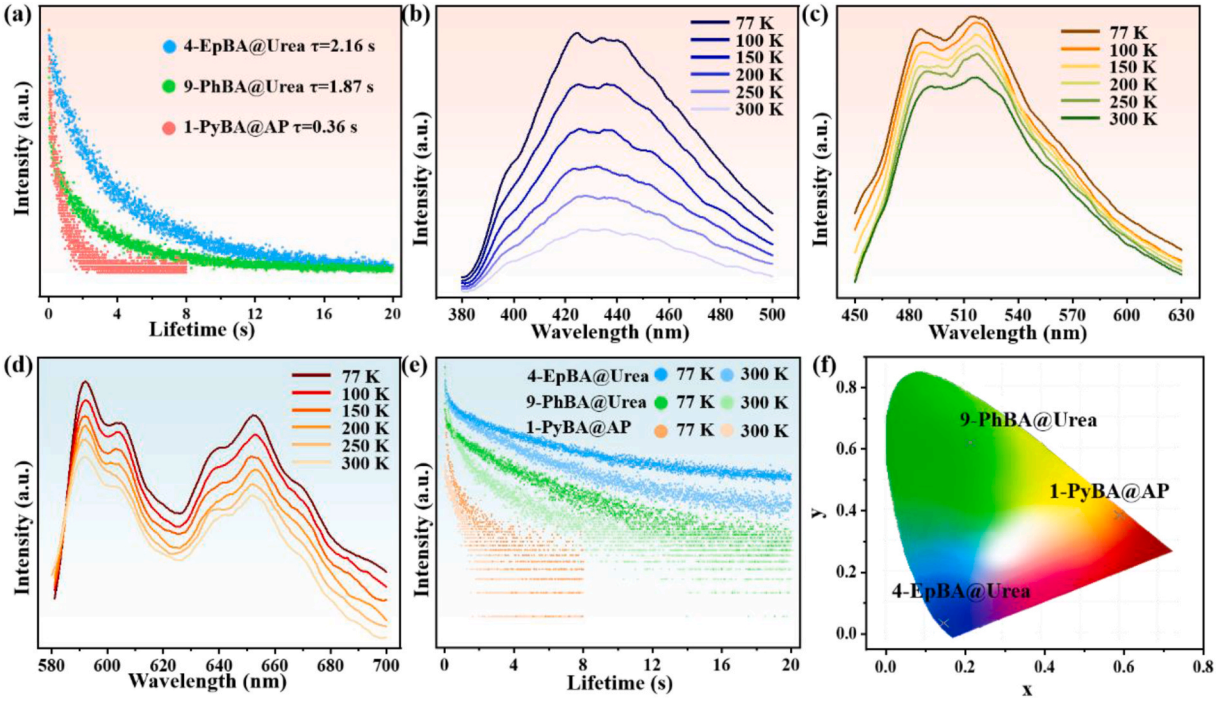

Fig. 5. a) Phosphorescence decay curves, b, c, d) Variable-temperature phosphorescence spectra, e) Phosphorescence decay curves at 77 k and 300 k, and f) CIE coordinates of 4-EpBA@Urea, 9-PhBA@Urea and 1-PyBA@AP.

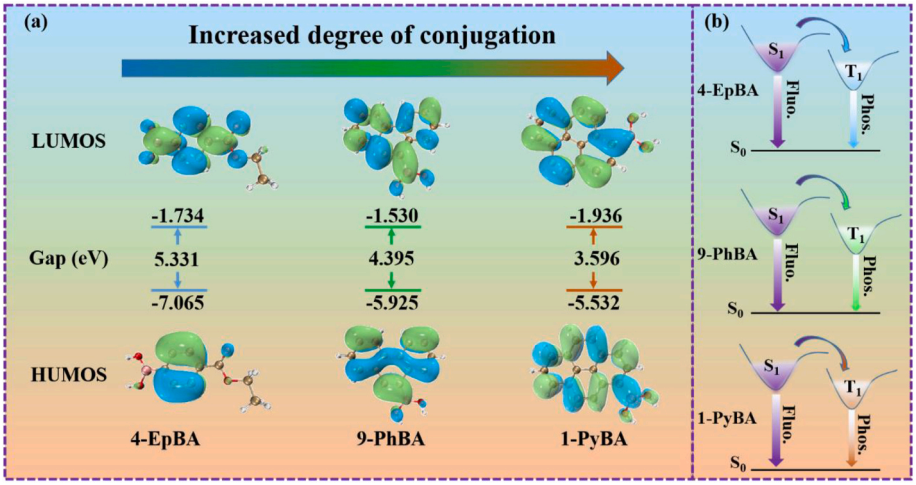

Fig. 6. a) The HOMO–LUMO electron cloud distributions and energy levels of 4-EpBA, 9-PhBA and 1-PyBA. b) The phosphorescent mechanism images of 4-EpBA@Urea, 9-PhBA@Urea and 1-PyBA@AP.

in a gradual redshift ofthe energy gap from the blue region, which is consistent with the observation that the 4-EpBA@Urea, 9-PhBA@Urea and 1-PyBA@AP with blue, green and orange phosphorescence colors. In addition, the ability of 1-PyBA@AP to generate orange phosphorescence compared to 1-PyBA@Urea is also an attractive phenomenon. Firstly, in the UV absorption spectrum, it is observed that 1-PyBA@Urea has no obvious absorption peaks in the region of 300–400 nm. However, the generation of orange RTP by CDs derived from 1-PyBA as a precursor requires energy absorption in the region around 317 nm (S1 = 3.9079) [31] to satisfy the energy level transition for 1-PyBA@Urea phosphorescence emission, and therefore 1-PyBA@Urea cannot generate orange RTP. Apparently, 1-PyBA@AP has significant energy absorption in the region of 300–400 nm to create orange phosphorescence emission. This is mainly attributed to the fact that the urea matrix is able to produce more gases during pyrolysis compared to the AP matrix resulting in a more loose matrix structure, and therefore less restriction of the growth of CNQDs and a larger spacing between the CNQDs in the urea matrix compared to the AP matrix (as can be observed in the TEM image in Fig. 2). For CBNQDs derived with AP as the precursor matrix, the CBNQDs dispersed in the B_2O_3 matrix were more densely, resulting in a small spacing between the CBNQDs, the higher degree of discrete π-orbital interactions and the enhanced π-bond conjugation, leading to a smaller energy required for the π - π* transition. Therefore, the absorption spectrum is significantly red-shifted to produce orange phosphorescence emission after the UV light was turned off.

Since 4-EpBA@Urea, 9-PhBA@Urea and 1-PyBA@AP exhibit different phosphorescence emission properties under UV light irradiation, they can be applied in advanced anti-counterfeiting and optical information storage. As shown in Fig. 7a, the anti-counterfeiting patterns of “bird” and “rose” were prepared by screen printing process. It can be observed that 4-EpBA@Urea shows the blue color of “bird” and “rose” after the UV light of 254 nm is turned off. In addition, green and

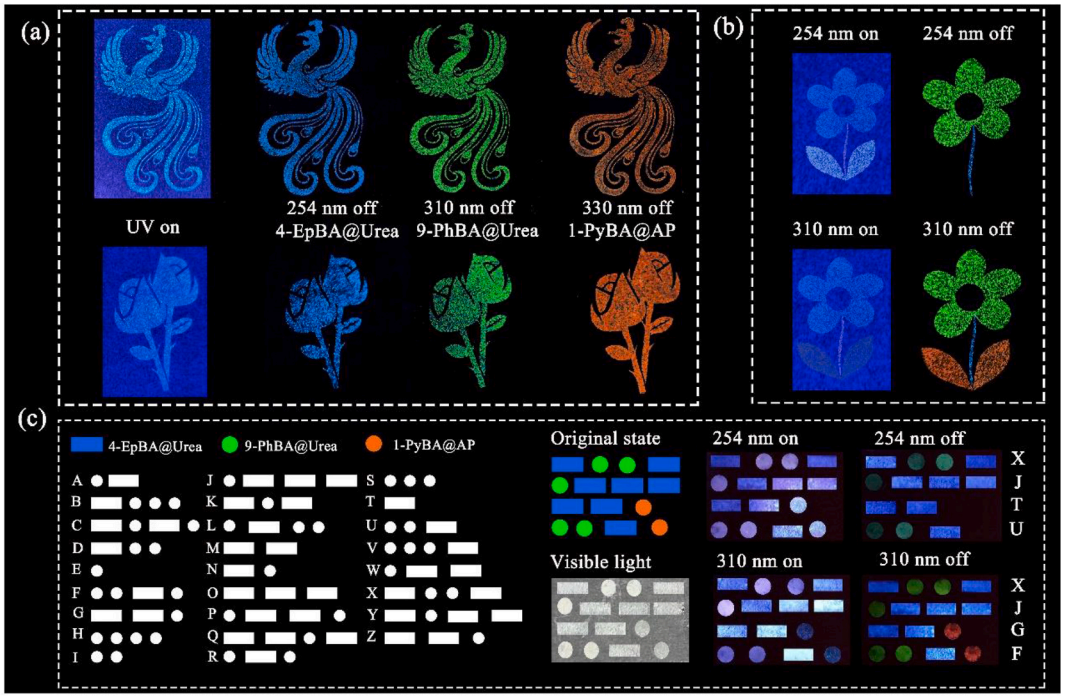

Fig. 7. a, b) Application of anti-counterfeiting patterns for 4-EpBA@Urea, 9-PhBA@Urea and 1-PyBA@AP. c) Morse code table with decoded image information under different light source excitations.

orange "bird" and "rose" patterns were observed in 9-PhBA@Urea and 1-PyBA@AP, respectively, after the UV light of 310 nm and 330 nm were turned off. Further, utilizing the property that 1-PyBA@AP does not produce any phosphorescence emission under excitation at 254 nm, however, it is capable of rendering 4-EpBA@Urea, 9-PhBA@Urea, and 1-PyBA@AP to generate blue, green, and orange phosphorescence, respectively, under excitation at 310 nm, the advanced anti-counterfeiting pattern was designed. As shown in Fig. 7b, "branches", "flowers" and "leaves" were printed on the substrate using 4-EpBA@Urea, 9-PhBA@Urea and 1-PyBA@AP as pastes, respectively. After the excitation light source of 254 nm is turned off, only blue "branches" and green "flowers" can be seen, but after the excitation light source of 310 nm is turned off, not only can we see blue "branches" and green "flowers", but also orange "leaves". In addition, optical information storage is also an important application in the field of RTP materials, nowadays. The information storage based on the Morse code is achieved by representing "dots" or "dashes" using 4-EpBA@Urea, 9-PhBA@Urea and 1-PyBA@AP, respectively. Fig. 7c illustrates a code array, consisting of the three materials on the same black background. Decoding with a 254 nm UV light source the message is "XJTU", while decoding with a 310 nm UV light source the message is "XJGF".

3. Conclusion

In conclusion, we successfully embedded CDs into the tri-*s*-triazine skeletons and B_2O_3 matrix by pyrolyzing precursor molecules with different conjugation degrees with urea and AP, respectively, achieving blue, green and orange phosphorescence emission. The phosphorescence lifetimes of the blue, green and orange RTP CDs were 2.16, 1.87 and 0.36 s, respectively, which were at a high level among the RTP CDs. In the interaction of covalent bonds such as O–H, N–C═N, and B–O, the surface functional group rotation of CDs is restricted, suppressing the nonradiative transition and successfully generating phosphorescence emission in tri-*s*-triazine and B_2O_3 matrices. On the one hand, with the increase of 4-EpBA@Urea, 9-PhBA@Urea and 1-PyBA@AP conjugation resulting in a red-shift of the phosphorescence emission spectra. On the other hand, since pyrolysis of urea generates a large amount of gases causing the matrix structure to be loose and the mutual spacing between CNQDs to increase, the distribution of CBNQDs with AP as the precursor matrix is more densely distributed compared with urea matrix, resulting in the higher degree of discrete π orbital interactions and conjugation, and the lower energy required for the π-π* transition. Therefore, 1-PyBA@AP has a significant red-shift in the absorption spectrum compared to 1-PyBA@Urea and is able to achieve orange phosphorescence emission after UV light excitation. Finally, based on the excellent color phosphorescence properties of 4-EpBA@Urea, 9-PhBA@Urea and 1-PyBA@AP, we successfully applied the prepared samples to advanced anti-counterfeiting and optical information storage, and this work also provides a new idea for the realization of the preparation of colorful RTP CDs composites.

CRediT authorship contribution statement

Qing Yao: Writing – original draft. **Yuan Wang:** Resources. **Minqiang Wang:** Writing – review & editing. **Nikolai V. Gaponenko:** Resources. **Zheyuan Da:** Data curation. **Jindou Shi:** Investigation. **Chen Zhang:** Data curation. **Junnan Wang:** Data curation.

Declaration of competing interest

The authors declare that they have no known competing financial interests or personal relationships that could have appeared to influence the work reported in this paper.

Data availability

No data was used for the research described in the article.

Acknowledgements

This work was supported by the National Key R&D Program of China (2022YFE0122500 and 2019YFB1503200), National Natural Science Foundation of China (NSFC, 52161145103 and 61774124), and 111 Program (No. B14040), and Shaanxi Provincial Key Research and Development Program (No.2021GXLH-Z-084), and the Natural Science Basic Research Program of Shaanxi (No. 2019JLP-18).

Appendix A. Supplementary data

Supplementary data to this article can be found online at https://doi.org/10.1016/j.mtchem.2024.102199.

References

[1] C.M. Tonge, N.R. Paisley, A.M. Polgar, K. Lix, W.R. Algar, Z.M. Hudson, Color-tunable thermally activated delayed fluorescence in oxadiazole-based acrylic copolymers: photophysical properties and applications in ratiometric oxygen sensing, ACS Appl. Mater. Interfaces 12 (2020) 6525–6535.
[2] Y. Su, S.Z.F. Phua, Y. Li, X. Zhou, D. Jana, G. Liu, W.Q. Lim, W.K. Ong, C. Yang, Y. Zhao, Ultralong room temperature phosphorescence from amorphous organic materials toward confidential information encryption and decryption, Sci. Adv. 4 (2018) eaas9732.
[3] H. Hu, J. Li, X. Gong, Hour-level persistent multicolor phosphorescence enabled by carbon dot-based nanocomposites through a multi-confinement-based approach, Small 20 (2023) 2308457.
[4] H.-T. Feng, J. Zeng, P.-A. Yin, X.-D. Wang, Q. Peng, Z. Zhao, J.W.Y. Lam, B.Z. Tang, Tuning molecular emission of organic emitters from fluorescence to phosphorescence through push-pull electronic effects, Nat. Commun. 11 (2020) 2617.
[5] B. Wang, Z. Sun, J. Yu, G.I.N. Waterhouse, S. Lu, B. Yang, Cross-linking enhanced room-temperature phosphorescence of carbon dots, Smartmat 3 (2022) 337–348.
[6] X. Yang, G.I.N. Waterhouse, S. Lu, J. Yu, Recent advances in the design of afterglow materials: mechanisms, structural regulation strategies and applications, Chem. Soc. Rev. 52 (2023) 8005–8058.
[7] X. Li, M. Rui, J. Song, Z. Shen, H. Zeng, Carbon and graphene quantum dots for optoelectronic and energy devices: a review, Adv. Funct. Mater. 25 (2015) 4929–4947.
[8] Y.-C. Liang, S.-S. Gou, K.-K. Liu, W.-J. Wu, C.-Z. Guo, S.-Y. Lu, J.-H. Zang, X.-Y. Wu, Q. Lou, L. Dong, Y.-F. Gao, C.-X. Shan, Ultralong and efficient phosphorescence from silica confined carbon nanodots in aqueous solution, Nano Today 34 (2020) 100900.
[9] M. Liu, Z. Liu, Z. Wen, N. Yu, D.K. Macharia, M. Zhu, Z. Chen, N-doped carbon-quantum-dot-integrated colorimetric system for visible photoprinting and oxygen sensing, Adv. Opt. Mater. 12 (2024) 2302787.
[10] J. Li, H. Zhao, X. Zhao, X. Gong, Boosting efficiency of luminescent solar concentrators using ultra-bright carbon dots with large Stokes shift, Nanoscale Horizons 8 (2022) 83–94.
[11] F. Yan, J. Li, X. Zhao, X. Gong, Unveiling unconventional luminescence behavior of multicolor carbon dots derived from phenylenediamine, J. Phys. Chem. Lett. 14 (2023) 5975–5984.
[12] Y. Zhang, S. Lu, Lasing of carbon dots: chemical design, mechanisms, and bright future, Chem 10 (2024) 134–171.
[13] S. Nakamura, D. Matsumaru, G. Yamahata, T. Oe, D.-H. Chae, Y. Okazaki, S. Takada, M. Maruyama, A. Fujiwara, N.-H. Kaneko, Universality and multiplication of gigahertz-operated silicon pumps with parts per million-level uncertainty, Nano Lett. 24 (2023) 9–15.
[14] Y. Liu, D. Chao, L. Zhou, Y. Li, R. Deng, H. Zhang, Yellow emissive carbon dots with quantum yield up to 68.6% from manganese ions, Carbon 135 (2018) 253–259.
[15] Y. Zhang, L. Chen, B. Liu, S. Yu, Y. Yang, X. Liu, Multicolor afterglow carbon dots: luminescence regulation, preparation, and application, Adv. Funct. Mater. (2024) 2315366.
[16] F. Gu, X. Ma, Stimuli-responsive polymers with room-temperature phosphorescence, Chem. Eur J. 28 (2022) e202304131.
[17] P. Long, Y. Feng, C. Cao, Y. Li, J. Han, S. Li, C. Peng, Z. Li, W. Feng, Self-protective room-temperature phosphorescence of fluorine and nitrogen codoped carbon dots, Adv. Funct. Mater. 28 (2018) 1800791.
[18] B. Zhao, R. Yu, K. Xu, C. Zou, H. Ma, S. Qu, Z.a. Tan, Highly efficient carbon dot-based room-temperature fluorescence-phosphorescence dual emitter, J. Mater. Chem. C 9 (2021) 15577–15582.
[19] F. Liu, Z. Li, Y. Li, Y. Feng, W. Feng, Room-temperature phosphorescent fluorine-nitrogen co-doped carbon dots: information encryption and anti-counterfeiting, Carbon 181 (2021) 9–15.
[20] Y. Cheng, W. Fan, R. He, X. Meng, Q. Zhou, X. Ma, Y. Liu, Y. Shi, L. Zheng, Q. Cao, Naphthoic acid Derivatives@Boric acid based fast photo-activated room-

temperature phosphorescence materials with dynamic changed emission color, Adv. Opt. Mater. (2024) 2303017.
[21] J. He, Y. He, Y. Chen, X. Zhang, C. Hu, J. Zhuang, B. Lei, Y. Liu, Construction and multifunctional applications of carbon dots/PVA nanofibers with phosphorescence and thermally activated delayed fluorescence, Chem. Eur J. 347 (2018) 505–513.
[22] L. Mo, H. Liu, Z. Liu, X. Xu, B. Lei, J. Zhuang, Y. Liu, C. Hu, Cascade resonance energy transfer for the construction of nanoparticles with multicolor long afterglow in aqueous solutions for information encryption and bioimaging, Adv. Opt. Mater. 10 (2022) 2102666.
[23] W. Shi, J. Yao, L. Bai, C. Lu, Defect-stabilized triplet state excitons: toward ultralong organic room-temperature phosphorescence, Adv. Funct. Mater. 28 (2018) 1804961.
[24] J. Liu, H. Zhang, N. Wang, Y. Yu, Y. Cui, J. Li, J. Yu, Template-modulated afterglow of carbon dots in zeolites: room-temperature phosphorescence and thermally activated delayed fluorescence, ACS Mater. Lett. 1 (2019) 58–63.
[25] C. Lin, Y. Zhuang, W. Li, T.-L. Zhou, R.-J. Xie, Blue, green, and red full-color ultralong afterglow in nitrogen-doped carbon dots, Nanoscale 11 (2019) 6584–6590.
[26] Q. Li, M. Zhou, Q. Yang, Q. Wu, J. Shi, A. Gong, M. Yang, Efficient room-temperature phosphorescence from nitrogen-doped carbon dots in composite matrices, Chem. Mater. 28 (2016) 8221–8227.
[27] W. He, X. Sun, X. Cao, Construction and multifunctional applications of visible-light-excited multicolor long afterglow carbon dots/boron oxide composites, ACS Sustain. Chem. Eng. 9 (2021) 4477–4486.
[28] S. Cui, B. Wang, Y. Zan, Z. Shen, S. Liu, W. Fang, X. Yan, Y. Li, L. Chen, Colorful, time-dependent carbon dot-based afterglow with ultralong lifetime, Chem. Eng. J. 431 (2022) 133373.
[29] Z. Guan, Z. Tang, J. Zeng, J. Deng, Y. Zheng, H. Li, X. Liu, Molecular engineering enables multi-color room temperature phosphorescence of carbon dots composites derived in situ, facilitating their utilization for advanced information encryption, Adv. Opt. Mater. (2024) 2302820.
[30] B. Han, X. Lei, D. Li, Q. Liu, Y. Chen, J. Wang, G. He, Shallow traps in carbon nitride quantum dots to achieve 6.47 s ultralong lifetime and wavelength-tunable room temperature phosphorescence, Adv. Opt. Mater. 11 (2023) 2202293.
[31] Z. Li, S. Cao, Y. Zheng, L. Song, H. Zhang, Y. Zhao, Colorful ultralong room temperature phosphorescent afterglow with excitation wavelength dependence based on boric acid matrix, Adv. Funct. Mater. 34 (2024) 2306956.
[32] Y. Zheng, Q. Zhou, Y. Yang, X. Chen, C. Wang, X. Zheng, L. Gao, C. Yang, Full-color long-lived room temperature phosphorescence in aqueous environment, Small 18 (2022) 2201223.
[33] S.-Y. Song, K.-K. Liu, X. Mao, Q. Cao, N. Li, W.-B. Zhao, Y. Wang, Y.-C. Liang, J.-H. Zang, X. Li, Q. Lou, L. Dong, C.-X. Shan, Colorful triplet excitons in carbon nanodots for time delay lighting, Adv. Mater. 35 (2023) 2212286.
[34] J. Wen, Z. Zeng, B. Wang, J. Hong, Y. Chen, J. Zhang, J. Li, J. Jiang, Modulating hydrothermal condition to achieve carbon dots-zeolite composites with multicolor afterglow, Nano Res. 16 (2023) 7761–7769.
[35] Z.H. Zhang, K. Leinenweber, M. Bauer, L.A.J. Garvie, P.F. McMillan, G.H. Wolf, High-pressure bulk synthesis of crystalline $C_6N_9H_3$•HCl: a novel C_3N_4 graphitic derivative, J. Am. Chem. Soc. 123 (2001) 7788–7796.
[36] Z. Xing, K. Dong, N. Pavlopoulos, Y. Chen, L. Amirav, Photoinduced self-assembly of carbon nitride quantum dots, Angew. Chem. Int. Ed. 60 (2021) 19413–19418.
[37] H. Liu, X. Lv, J. Qian, H. Li, Y. Qian, X. Wang, X. Meng, W. Lin, H. Wang, Graphitic carbon nitride quantum dots embedded in carbon nanosheets for near-infrared imaging-guided combined photo chemotherapy, ACS Nano 14 (2020) 13304–13315.
[38] J. Zhou, Y. Yang, C.-y. Zhang, A low-temperature solid-phase method to synthesize highly fluorescent carbon nitride dots with tunable emission, Chem. Commun. 49 (2013) 8605–8607.
[39] B.H. Tran, K. Tieu, S. Wan, H. Zhu, S. Cui, L. Wang, Understanding the tribological impacts of alkali element on lubrication of binary borate melt, RSC Adv. 8 (2018) 28847–28860.
[40] T. Yuan, F. Yuan, X. Li, Y. Li, L. Fan, S. Yang, Fluorescence-phosphorescence dual emissive carbon nitride quantum dots show 25% white emission efficiency enabling single-component WLEDs, Chem. Sci. 10 (2019) 9801–9806.
[41] Y. Li, Q. li, S. Meng, Y. Qin, D. Cheng, H. Gu, Z. Wang, Y. Ye, J. Tan, Ultrabroad-band,white light emission from carbon dot-based materials with hybrid fluorescence/phosphorescence for single component white light-emitting diodes, Chin. Chem. Lett. 34 (2023) 107794.
[42] Q. Feng, Z. Xie, M. Zheng, Colour-tunable ultralong-lifetime room temperature phosphorescence with external heavy-atom effect in boron-doped carbon dots, Chem. Eng. J. 420 (2021) 127647.
[43] Y. Di, W. Liu, S. Shi, T. Wu, M. Wang, X. Liu, One-step synthesis of color-tunable carbon dots-based organic long persistent luminescence materials, Chem. Eng. J. 479 (2024) 147589.
[44] C. Zhang, H. Wang, X. Lan, Y.-e. Shi, Z. Wang, Modulating emission of nonconventional luminophores from nonemissive to fluorescence and room-temperature phosphorescence via dehydration-induced through-space conjugation, J. Phys. Chem. Lett. 12 (2021) 1413–1420.
[45] Z. Zhang, Z. Wang, X. Liu, Y.-e. Shi, Z. Li, Y. Zhao, Modulating emission of boric acid into highly efficient and color-tunable afterglow via dehydration-induced through-space conjugation, Adv. Sci. 10 (2023) 2300139.
[46] P.M. Burrezo, J.L. Zafra, J.T. López Navarrete, J. Casado, Quinoidal/aromatic transformations in π-conjugated oligomers: vibrational Raman studies on the limits of rupture for π-bonds, Angew. Chem. Int. Ed. 56 (2017) 2250–2259.
[47] K. Wan, Y. Zhai, S. Liu, J. Li, S. Li, B. Strehmel, Z. Chen, T.D. James, Sustainable afterglow room-temperature phosphorescence emission materials generated using natural phenolics, Angew. Chem. Int. Ed. 61 (2022) e202202760.
[48] J. Li, Y. Wu, X. Gong, Evolution and fabrication of carbon dot-based room temperature phosphorescence materials, Chem. Sci. 14 (2023) 3705–3729.
[49] S. Grimme, S. Ehrlich, L. Goerigk, Effect of the damping function in dispersion corrected density functional theory, J. Comput. Chem. 32 (2011) 1456–1465.